Ocean Engineering 165 (2018) 22–33

Contents lists available at ScienceDirect

Ocean Engineering

journal homepage: www.elsevier.com/locate/oceaneng

An experimental and non-dimensional study on the vertical temperature distribution of a sealed ship engine room fire

Jinhui Wang[a,*], Yu Jiao[a], Long Shi[b,**], Qimiao Xie[a], Guoqiang Li[c], Jiahao Liu[a], WeiJiong Chen[a], Shaogang Zhang[a]

[a] College of Ocean Science and Engineering, Shanghai Maritime University, Shanghai 201306, China
[b] Civil and Infrastructure Engineering Discipline, School of Engineering, RMIT University, GPO Box 2476, Melbourne, VIC 3001, Australia
[c] State Key Laboratory for Disaster Reduction in Civil Engineering, Tongji University, Shanghai 200092, China

ARTICLE INFO

Keywords:
Ship safety
Sealed engine room fire
Pool fire
Vertical temperature distribution
Non-dimensional analysis
Empirical model

ABSTRACT

Fire in a sealed ship engine room is different from open fires, while its suppression is critically important to the emergency rescue and structure safety for a ship. This study focused on the vertical distribution of temperature rise during a sealed engine room fire. A series of experiments were carried out to investigate fire behaviors in a reduced-scale sealed ship engine room with a dimension of 3 m (length) × 3 m (width) × 3.5 m (height). The results suggested that there are vertical temperature gradients of smoke layer, showing a little lower than those of open fires. The experimental results demonstrated that the time to reach the maximum temperature is different for smoke layers at various heights, while a lower height showed a relatively long delay time. The vertical gradient of temperature rise was found increasing with pool diameter where the gradient of temperature rise of a 30 cm pool fire is about 9 times of that of a 10 cm pool fire. Furthermore, an empirical model was developed to predict the vertical temperature rise distribution along the height at the time of the maximum temperature for sealed engine room fires.

1. Introduction

One of the most disastrous situations threatening passengers/occupants in ships and related constructions is fire, which comes with high risk and uncertainty (Kang et al., 2017; Salem, 2016; Su and Wang, 2013). In fire emergency circumstances of a ship, to close the burning engine room is a final-taken and efficient means to extinguish the fire, especially when the ship is at sea without any help or support. For this case, ship engine room is completely closed, and the fire will be eventually extinguished due to the lack of oxygen. Sealed engine room fire is a special type as it is isolated from the ambient environment. Smoke and combustion products released from fire sources cannot be exhausted outside, and no fresh air is entrained into ship engine room as well. As a result, fire behaviors in a sealed engine room then is distinctly different from those of open fires (Zhang et al., 2013a, 2013b, 2015; Yuan et al., 2014; Tatem et al., 1986; Li et al., 2011; Yang et al., 2013).

Temperature or temperature rise is one of the critical parameters regarding the fire characteristics, which is essential to address the smoke movement and related suppression measures. Based on temperature, the initiation, development and extinguishment stages of sealed fires can be identified accordingly (Wang et al., 2017; Yao et al., 2017; Yoon et al., 2010). If a sealed engine room fire cannot be suppressed directly by fire extinguishing system, one of the alternative measures is to seal the engine room and wait for its self-extinguishment (Pu, 2009). After sealing the engine room, fire can be suppressed when the oxygen concentration drops to a certain value. After the fire is extinguished, the right time to reopen the ship engine room is very important. This is because the engine room is rich of fuel and also under high-temperature conditions, so re-ignition even backdraft may occur after sudden fresh-air entrance (Trouve and Wang, 2010). More importantly, the influences of hot smoke on the engine room structure are worthy of being studied, especially on accurately identifying or predicting the failure location of the engine room structure, which is significant to the structural risk assessment or fire emergency rescue (Kim et al., 2017; Jin et al., 2016; Jin and Jang, 2015). Therefore, the temperature distribution of sealed engine room fires is a practically important research topic.

Previous studies regarding the temperature rise in compartment fires, especially for a building fire, has been studied for several years,

* Corresponding author.
** Corresponding author.
E-mail addresses: sunrise@mail.ustc.edu.cn (J. Wang), shilong@mail.ustc.edu.cn (L. Shi).

https://doi.org/10.1016/j.oceaneng.2018.07.018
Received 14 February 2018; Received in revised form 7 July 2018; Accepted 7 July 2018
Available online 11 July 2018

Nomenclature

$\propto$	proportional relationship	g	gravitational acceleration, m/s^2
χ	combustion efficiency	h	height of thermocouples, m
$\dot{m}$	average mass loss rate, g/s	D	diameter of pool fire, m
ΔH	heat of combustion, kJ/g	H	height of ship engine room, m
L	scale ratio	S	floor area of ship engine room, m^2
$\dot{Q}$	heat release rate, kW	$\Delta T(h)$	temperature rise at height of h, °C
$\overline{\dot{Q}}$	average heat release rate, kW	$\dot{Q}^*$	non-dimensional heat release rate
T_∞	ambient temperature, K	$\overline{\dot{Q}}^*$	non-dimensional average heat release rate
ρ_∞	density of ambient air, kg/m^3	$\Delta T(h)^*_{max}$	non-dimensional temperature rise at the time of maximum temperature
c_p	specific heat capacity of ambient air, kJ/kg·K	k	slope obtained from regression
		b	intercept obtained from regression

representative models such as M-Q-H method, F-P-A method, Beyler method, etc. (Walton et al., 2016). These models were developed based on the conservation of energy and mass for the gas phase inside the enclosure with openings or under well-ventilation. These models are typical zone models, including one-zone and two-zone models. The basic assumption of zone models is considered uniform for a one-zone model or the upper layer of the two-zone model. These models can predict the average temperatures which reflect the heat accumulation in the enclosure. Nevertheless, detailed temperature profiles are still a challenge of prediction. As we conduct the thermo-mechanical coupling analysis to assess the structural safety of ship engine room, the knowledge of the detailed temperature profiles is compulsory.

In the aspect of experimental study, Hu et al. conducted a series of fire experiments in a closed ship engine room and found that the temperature profile at the moment of self-extinction follows the Boltzmann distribution (Hu et al., 2010). Zhang et al. have investigated experimentally the vertical temperature distribution induced by an elevated fire in a ceiling vented ship compartment and found that the temperature of the upper layer was much higher than that of the lower layer (Zhang, 2014; Li et al., 2018). The stratification of the temperature was distinct including two regions of the hot upper layer and the cold lower layer according to the measured temperature. Additionally, Li and Chen have conducted experiments in a horizontally vented ship enclosure, smoke filled up the enclosure quickly after ignition and temperature seemed to increase gradually with height in most cases, which was quite similar to some forced-ventilation compartment fires (Li, 2010; Chen, 2011).

In numerical simulation studies, some studies focused on sealed engine room fires were based on numerical modeling (Su et al., 2012; Wang et al., 2013; Salem, 2013; Bonte et al., 2013; Jia et al., 1997; Sekret et al., 2013). The temperature distribution, volume fractions of gas species and thickness of smoke layer were investigated numerically. Another challenge is that the zone modeling, which divides the whole space into several vertical layers, may be no longer applicable to sealed engine room fires (Yuan et al., 2014).

In addition, some theoretical models have been developed regarding the prediction of temperatures in sealed engine rooms. A five-zone theoretical model (Tatem et al., 1986) was developed to predict the temperature in a gas-tight enclosure, which was based on the assumption that the combustion products and evaporated fuel are fully mixed. Another way of simplification is to consider a unified temperature for smoke layers (Li et al., 2011; Yang et al., 2013). Computational fluid dynamics models (Zhang et al., 2015) were also utilized to address the situation. However, there is still a gap between the prediction and experiments. Research efforts are especially needed from the experimental aspects.

Based upon the above analysis, previous studies have largely focused on the ship fires in ventilated or unsealed engine rooms, leaving very few studies on fully sealed engine room fire. The purpose of this study mainly focuses on the vertical distribution of temperature rise induced by fire in a sealed ship engine room. There are three main sections. The first section presents an introduction of a reduced-scale experimental rig. The second section focuses on experimental results and analysis including average mass loss rate, average heat release rate and vertical temperature rise. The third section conducts a dimensionless analysis of vertical temperature distribution at the time of maximum temperature and proposes a mathematical model.

2. Experimental methodology

A bench-scale ship engine room model was built to conduct a series of experiments, as shown in Fig. 1. In this figure, a transparent front-wall was used only to show the inside items, which does not mean that the wall of the testing engine room is transparent. To facilitate the observation of fire burning behaviors in a sealed ship engine room during experimental tests, several circular holes are set as experimental observation windows in the front and back walls, which are made of quartz glass and can stand for a high temperature of 600 °C. This ship engine room model consists of four parts, namely testing engine room, temperature measurement system, data collection system, and weighing device. The details of each part are introduced as follows:

(1) Testing engine room. Previous experimental studies were much focused on a relatively smaller engine room model than the one used in this study. For example, Zhang et al., 2013a, 2013b studied the characteristics of pool fire in two closed compartments, while one is 3 m (Length) × 3 m (Width) × 1.95 m (Height) and the other is 1 m (Length) × 1 m (Width) × 0.75 m (Height). The dimension of the current testing engine room is 3 m (Length) × 3 m (Width) × 3.5 m (Height), as shown in Fig. 1.

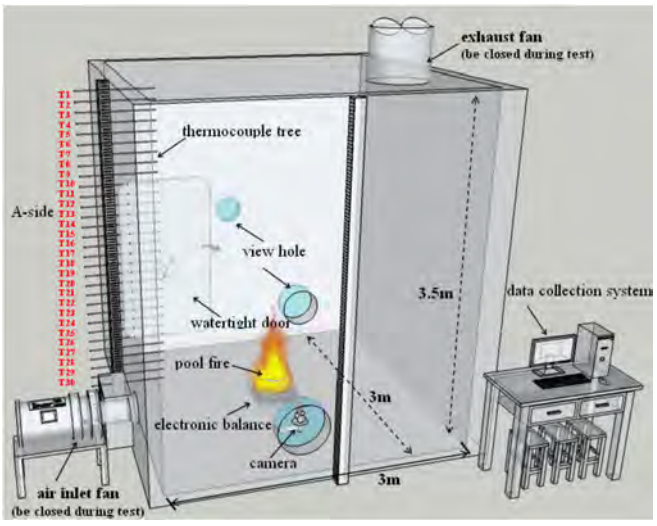

Fig. 1. Schematic diagram of the ship engine room test model.

The design of this engine room was following the Chinese code CB/T3368-2013 (CB/T3368-2013, 2013). The wall was made of Rockwool steel sandwich panel with a middle layer of 20 mm Rockwool, while the external and internal layers were 4 mm and 1.5 mm carbon steel panels, respectively. The internal lining was made by 25 mm alumina-silica insulation board. The floor was also made by the sandwich panel, while its bottom, middle and top layers were made of 1.5 mm carbon steel, 20 mm Rockwool, and 4 mm carbon steel, respectively. A 1.5 mm anti-slip panel was used at the top of the floor.

A quick-open watertight door was used with good airtightness. A rotating handle and water seal strips were used to ensure the door can be fully sealed to avoid leakage. The designs of related insulation for the door were following CB/T3368-2013 (CB/T3368-2013, 2013), with a dimension of 1.6 m (Length) × 0.8 m (Width) × 0.04 m (Depth).

(2) Temperature measurement system. K-type thermocouples were employed to record the temperature history at different heights, which also represent the time-varying temperature of the smoke layer.

The thermocouple tree on Side A, where each thermocouple is mounted with 30 cm depth into the ship engine room, is located vertically along the centerline of A-side wall. Here, each thermocouple being inserted into the engine room with 30 cm depth is to avoid the effects of the anti-buoyant jet behavior on the temperature measurement. Thirty measured spots are arranged vertically from 3.4 m to 0.5 m heights with an interval of 0.1 m, which are labeled by T1 to T30, respectively. The measuring temperature range of these thermocouples is about 600 °C, which is enough for the measurement of smoke

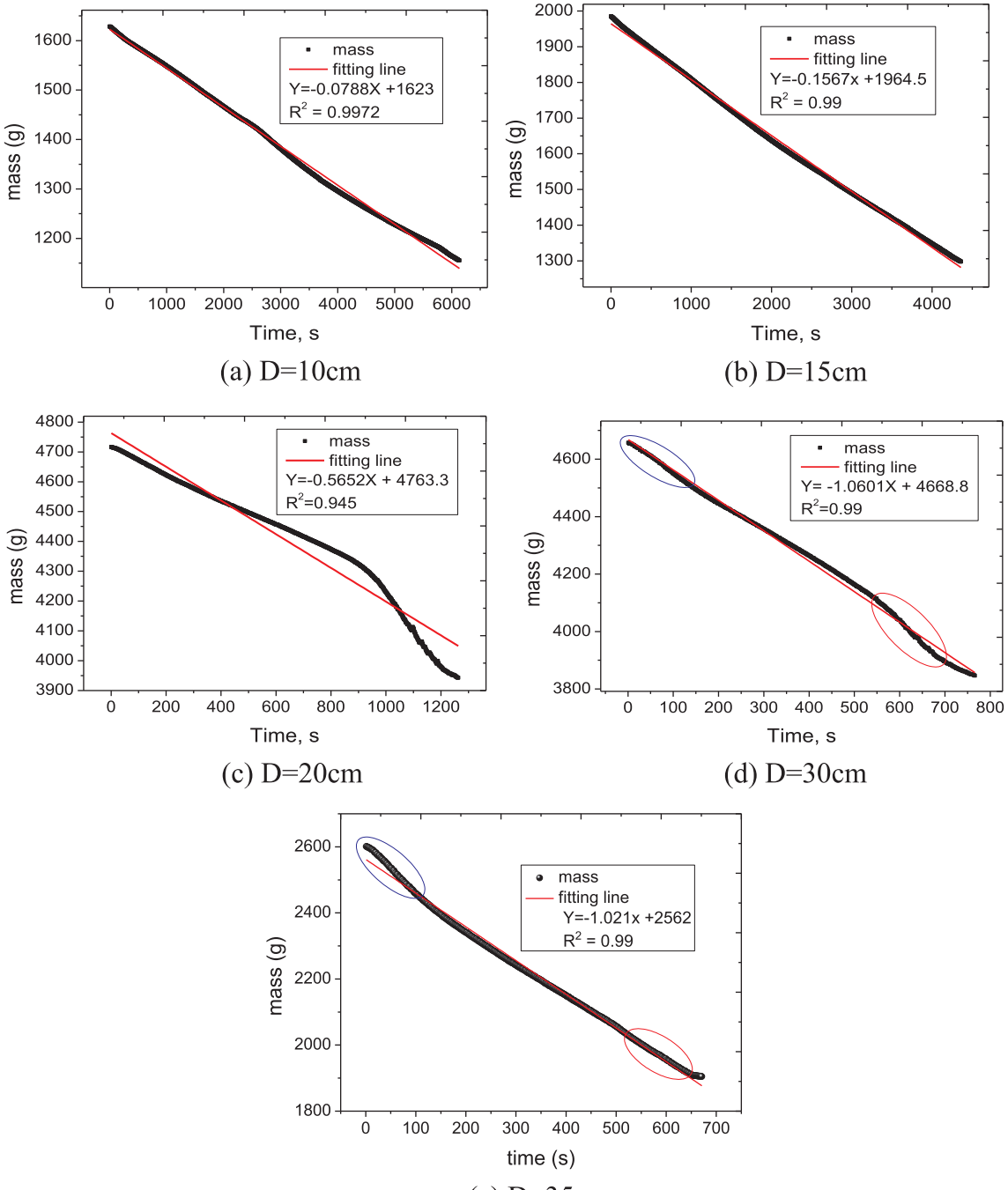

Fig. 2. Mass loss of liquid pool fire with a diameter of: (a) 10 cm; (b) 15 cm; (c) 20 cm; (d) 30 cm; and (e) 35 cm.

temperature in this study. Their response time is 1 s, namely with a measurement frequency of 1 Hz.

(3) Data collection system. The computer with a special configuration software system installed can automatically record the data taken during the experiments, including temperature history and mass loss. The sampling frequency of the data collection system is also 1 Hz. The data collection includes the temperature measurement data of those 30 thermocouples mentioned above and the mass loss of fuel taken by the electronic balance.
(4) Weighing device. An electronic weighing device called ES-5000 was utilized to record the total mass of liquid fuel and the container (fuel pan) in real-time. The maximum reading is 5 kg with an accuracy of 0.01 g. The sampling frequency of this weighing device is 1 Hz.

Liquid pool fire is one of the most common types of ship fire as ships usually contain large amount liquid, such as lubrication oil, machine oil and fuel oil. Generally, the liquid pool could happen due to the leakage accident from the vessel or pipe during transportation or storage. The liquid pool can spread under the gravity or floor with slope, and liquid pool with different depths can be formed under different scenarios. It can be then ignited by high-temperature contact or direct flame, which can be classified as Class B fire.

The commonly used oil for a ship would be fuel oil or hydraulic oil, which is basically hydrocarbon. N-heptane as a commonly used hydrocarbon fuel is a stable burning source which has been largely used in previous fire experiments (Hu et al., 2005; Utiskul et al., 2005). In this study, to be consistent with previous studies, n-heptane was then used as well. For the sake of simplicity, the oil pool fires used in experiments were placed in the center of the engine room floor.

The depths of the oil pools with different diameters were all 10 cm. The diameters of liquid fuel pan were 10, 15, 20, 30, and 35 cm, respectively. Except for 10 cm pool fire, the initial amount of fuel in each test was sufficient to maintain combustion under fully sealed conditions. The use of 10 cm pool fire was taken preliminarily to identify the type of extinguishment, namely oxygen-based or fuel-based. As stated above, the main purpose of this study is to conduct related experiments to simulate the case of fire self-extinguishing by sealing the ship engine room. In experiments, we can open or close the air inlet and outlet by adjusting the solenoid valve control. The air inlet and outlet of the testing engine room are both closed simultaneously after ignition. Then, both the outlet and inlet air fans were turned off as well during the whole experimental period. Meanwhile, after the experiments completed, the smoke exhaust is done by opening the outlet and launching the fan. Then, we open the air inlet and the air inlet fan as the smoke temperature drops to about 100 °C.

3. Results and discussion

3.1. Average mass loss rate

Burning process is accompanied by chemical reactions which consume both fuel and oxygen. For open fires, it is usually considered that only the evaporated fuel is involved in the chemical reactions. Under the situation, the burning rate of the liquid fuel is equal to its evaporation rate. A higher burning rate represents more released heat from the fire source, and the released heat during a unit time period is then defined as heat release rate.

In sealed compartment fires, environmental conditions of combustion, such as pressure, air density, and oxygen concentration, change frequently along the burning process, while the burning rate changes very complexly. Under low-oxygen conditions, not all evaporated fuel can be involved in the chemical reactions during the burning process, so the burning rate of the fuel is less than mass loss rate. This explains why the burning rate of fuel in sealed spaces is smaller than those in open spaces. It is also known from the previous study (Tatem et al., 1986) that the rising temperature can increase the evaporation rate of the liquid fuel. Eventually, the dropping oxygen concentration will reduce the evaporation rate through its influence on the flame height and air entrainment rate.

The mass of liquid fuel was measured during the whole experimental period. The fuel mass loss history in the time period from ignition to extinguishment is shown in Fig. 2 by plotting fuel mass versus the time. For each test, it is observed the mass shows a good linear relationship with the time. The fitting lines were linearly obtained for each scenario with a goodness of fit of more than 0.9 as illustrated in Fig. 2. Through linear regression analysis, the absolute value of the slope from the fitting line is the average mass loss rate during the whole burning process. It is easily seen that the average mass loss rate increases with a bigger diameter of a pool fire. The average mass loss rate increases from 0.078 to 1.06 g/s when pool diameter increases from 10 to 30 cm.

It needs to be noticed that the average mass loss rates are nearly the same for 30 and 35 cm pool fire. The possible reason for this is as follows. It can be seen from Fig. 2(d) and (e) that the mass loss rate of 30 cm pool fire at the later stage in the red circle increases than that in the previous stage. Seen from the recorded experimental video, it can be hypothesized that the temperature of the pool wall increases, resulting in a relatively rapid heat transfer that the liquid fuel inside the pool then goes to boiling. Under this circumstance, a part of the liquid fuel then splashes out of the pool, resulting in ghost fire when they go through the evaporation process. For the 35 cm pool fire, the mass loss rate at the early stage is relatively larger than that of the 30 cm pool fire. But in the later stage, the splashed liquid fuel is relatively less as comparing to that of the 30 cm pool fire. Therefore, with the combined effects, the 30 cm and 35 cm pool fires show a similar average mass loss rate during the whole combustion stage. As the average mass loss rate is dependent on combustion during early and late stages, the similar average mass loss rate does not mean that the 30 and 35 cm pool fires show a similar transient burning rate. Further research should be carried out in the future.

It should be noticed that for the pool fires with over 15 cm diameter ghost fire can be observed at the later stage of combustion or when the burning approaches to extinguishment. Ghost fire is a special kind of fire phenomenon. Sugawa et al. (1991) firstly found the ghost fire behavior in a poorly-ventilated compartment fire test, in which he concluded that ghost fire can occur in a poorly ventilated or sealed space that the oxygen concentration is much lower than the ambient level. So at the later stage of fire burning, due to the lack of oxygen, the flame can detach completely from the fuel source. The mechanism of ghosting is not yet fully understood. Fig. 3 shows the ghost fire under 30 cm pool fire pan. It is important to know that the ghost fire obviously has a significant impact on mass loss rate and spatial temperature distribution. For example, the mass loss rate with both 20 and 30 cm pool fire pans fluctuate obviously when approaching to the end. Some previous studies have also reported the same phenomenon for sealed engine room fires (Li et al., 2010). Furtherly, the ghost fire also affects the mass loss rate and temperature distributions in the sealed engine room.

It can be known from Fig. 2 that the average mass loss rate for 10, 15, 20, 30 and 35 cm diameter pools are about 0.01, 0.008, 0.018,

Fig. 3. Ghost fire for 30 cm pool fire.

0.015 and 0.011 kg/m^2·s, respectively. The average mass loss rate shows an increasing trend but the increase is not significant when the diameter rises from 10 to 35 cm. The free burning pool fire is then showing different behaviors. Chen et al. (2011) conducted an n-heptane pool fire test in a large test hall (12 m cube hall). The burning rates showed an increasing trend with pool diameter, and for pool diameters of 10, 14.1 and 20 cm the values are 0.012, 0.015, and 0.017 kg/m^2·s, respectively. The burning rates of sealed fire show relatively smaller values (averagely about 24% less) when compared to those under the condition of free burning. This is probably because of the burning in a sealed room is mainly dominated by oxygen supply, but for free burning pool fire, it is controlled by fuel supply.

3.2. Average heat release rate

Generally, for a compartment fire, heat release rate (*HRR*) in previous studies is usually used as a significant indicator to represent fire size. It cannot be measured directly, which is calculated based on oxygen consumption (Jin, 2012). For open fires or compartment fires with an opening, the oxygen level of released smoke from fire source can be directly measured to determine the *HRR* of a fire, such as using ISO 9705 full-scale test platform or cone calorimeter (Shi and Chew, 2012). But for a sealed engine room, it is very difficult to measure the oxygen level of released smoke from the fire source in a sealed compartment directly. As a result, there is no an instrument that can be used for direct measurement at present.

As for a sealed engine room fire, the oxygen level in the engine room at the early stage of a fire is sufficient, and the combustion is a fuel-controlled burning. With the development of combustion process, the oxygen concentration in the engine room keeps decreasing as there is no fresh air supply. Subsequently, it evolved into a limited combustion state and eventually leads to the occurrence of fire self-extinguishment due to oxygen deficiency. It is known that *HRR* is closely related to the real-time oxygen concentration around the fire source. So during the whole combustion process, *HRR* for a sealed engine room fire is not constant but transient even does not has a relative steady-combustion stage.

In this study, in order to characterize the fire size of an engine room fire, an average *HRR* in whole combustion period is employed to represent the fire size. The average *HRR* is calculated by averaging the total released heat over the whole burning period. As the total released heat is an integral of *HRR* over the whole burning process, the average *HRR* is therefore proportional to the average mass loss rate of fuel,

$$\bar{Q} = \chi \dot{m} \Delta H \tag{1}$$

where χ is the average combustion efficiency; $\dot{m}$ is the average mass loss rate during the whole combustion stage, g/s; and ΔH is the heat of combustion of fuel, kJ/g, which is 44.6 kJ/g for n-heptane in this study (Ma, 2015).

Generally, combustion efficiency is defined as the ratio of the actual heat release from fuel combustion to the complete heat of combustion, which is used to determine the completeness of burning. It also means that the ratio of the heat released in a combustion reaction to the theoretically complete combustion heat. For an open fire, the concentrations of oxygen are assumed to keep the same all the time. The combustion efficiency is herein considered as a constant under this circumstance. However, for a sealed engine room fire, the burning process is much complicated as the oxygen concentration keeps decreasing along the time, which results in heat accumulation, burning products and repeated air entrainment. The combustion efficiency is therefore different from that of open fires. With the change of combustion efficiency, the heat released and temperature distribution in the ship engine room are also changed accordingly.

In Zhang's studies (Zhang et al., 2013a), the combustion efficiency of fuel combustion in a closed compartment with elevated fires was systematically investigated using two different methods including oxygen depletion method (ISO 19703) and the equation deduced from *HRR* by oxygen consumption method. The experimental results showed that the combustion efficiency in a sealed compartment dropped gradually as the oxygen concentration decreases. It also says that in the whole burning process the combustion efficiency is not a constant and changes along the time. Furthermore, the average combustion efficiency in the whole process of combustion was also investigated. It was obtained as approximately 0.742 for fire centrally located with 22 cm high in the engine room, which is approximately the same as the situation of this study. Additionally, in Jin's work (Jin, 2012), based on both numerical and experimental study on sealed compartment fires, it was suggested an average combustion efficiency of 0.75 in sealed compartment fires in which the numerical results obey reasonably well with the experiments. Based upon the above analysis, the average combustion efficiency was approximately 0.75 for a sealed ship engine room fire in this study.

The average *HRR* can be calculated based on the average mass loss rate measured in the above section, which is listed in Table 1. It is known that the average *HRR* increases with the pool diameter. This is because for a bigger pool diameter the heat release increases with a bigger burning area. For a fixed effective heat of combustion, there is a linear relationship between the heat release rate and mass loss rate (Shi and Chew, 2013). The trend of *HRR* of the sealed pool fire is then similar to that of mass loss rate for a specific fuel. Roh et al. (2008) also obtained a similar trend but relatively smaller values through a reduced-scale test, namely a sealed tunnel with a dimension of 0.4 m (Height) × 0.4 m (Width) × 10 m (Length). The *HRR* increases from 2.23 to 10.95 kW when the pool size rises from 4.5 to 8.5 cm. The difference is probably because of the volume of the space.

Generally, the reduced-scale experiments are usually conducted based on the similarity principle. In this study, a 1/4–1/8 reduced-scale model comparing to full-scale model is used. In accordance with dynamic similarity, the Froude number remains the same for various-scaled models (Liu et al., 2004). The heat release rate is proportional to the scale ratio to a power of 5/2,

$$\dot{Q} \propto L^{5/2} \tag{2}$$

In Eq. (2), L is the scale ratio, which is 1/4–1/8 for this study. From

Table 1
Experimental conditions and average heat release rate for pool fire with different diameters.

Pool diameter D (cm)	Average mass loss rate, $\dot{m}$(g/s)	Average heat release rate, $\bar{Q}$(kW)	Ambient temperature	Relative humidity	Net weight of pool (g)	Gross weight before ignition (g)	Gross weight after the experiment (g)	Self-extinguished[a]
10	0.0788	2.636	16 °C	55%	1155.33	1628.6	1155.33	No
15	0.1567	5.242	21 °C	50%	1134.36	1984.6	1298.15	Yes
20	0.5652	18.906	16 °C	46%	3779.33	4716.04	3942.88	Yes
30	1.0601	35.460	14 °C	60%	3637.80	4657.34	3846.24	Yes
35	1.0208	34.146	19 °C	67%	1079.38	2600.76	1904.85	Yes

[a] Note: Self-extinguished means that fire extinguished due to lack of oxygen. It can be found that there is some liquid fuel remaining in the pool pan at the end of the experiment.

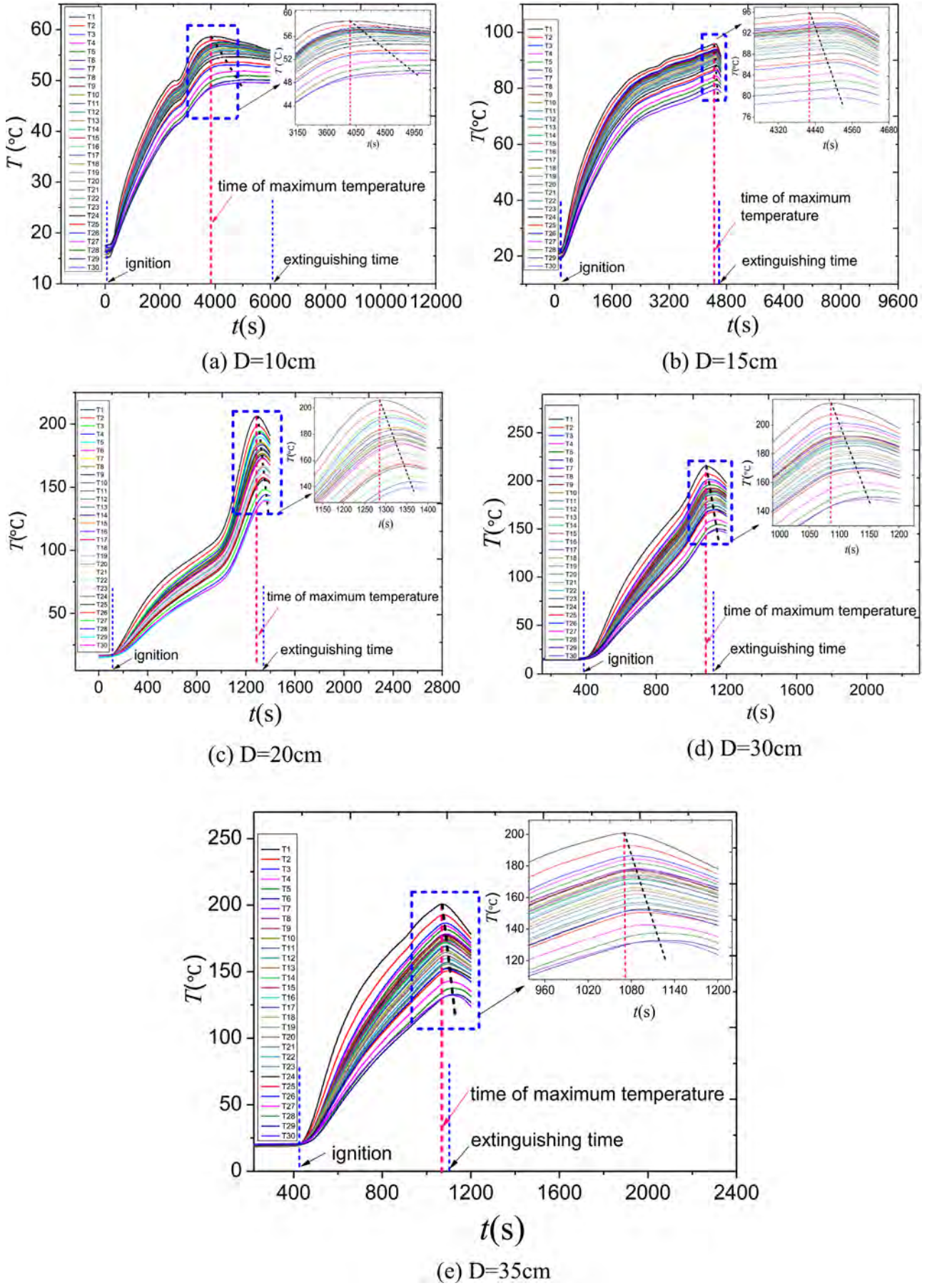

Fig. 4. Temperatures at different heights for pool fires with various diameters.

Table 1, it is seen that the maximum *HRR* for all the tests is about 34.1 kW and the minimum *HRR* is 2.6 kW. According to Eq. (2), the minimum *HRR* of 2.6 kW is corresponding to a fire of 470.7 kW in a maximum full-scale test, and the maximum *HRR* in our experiments also corresponds to a maximum full-scale *HRR* of 34.1 kW/(1/8)$^{5/2}$ = 6155 kW with a sealed engine room of 24 m (length) × 24 m (width) × 28 m (height) of a large cargo ship, such as container ships.

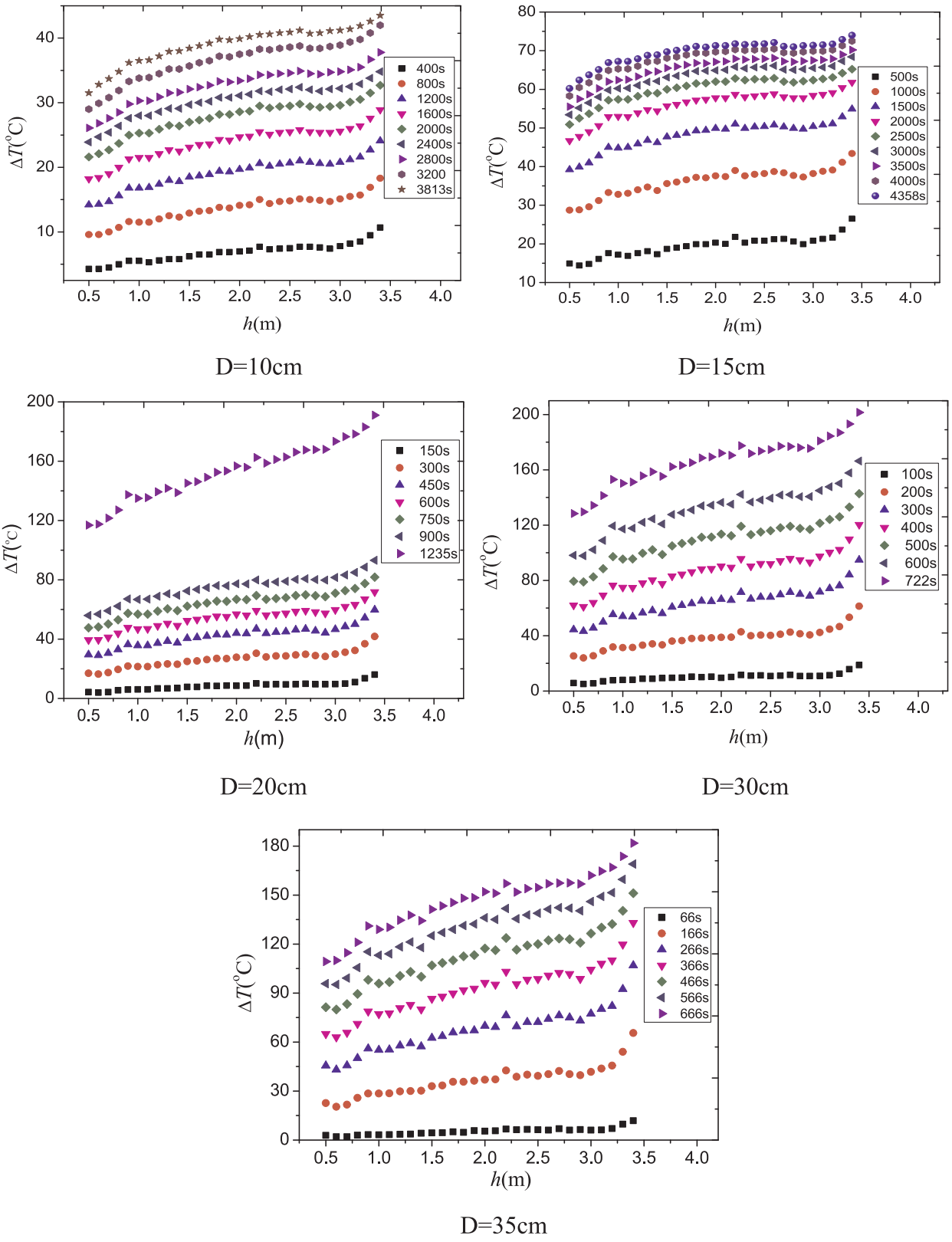

Fig. 5. Vertical temperature distributions versus time for pool fires with various diameters.

3.3. Vertical temperature rise

For various diameter pool fires, the temperature histories at different heights were recorded by thermocouples, as shown in Fig. 4. It is easily seen that the temperature rise increases with a bigger pool. This is because, under a bigger pool, the *HRR* of pool fire increases due to more released heat, resulting in a higher temperature of smoke at different heights. Additionally, the times reaching the maximum temperature are different under various pool fires. The details are illustrated in the subgraphs of Fig. 4. It can be seen that the time to reach the maximum temperature is different for smoke layers at various heights, and a lower height shows a relatively long delay time, especially for those small pool fires. As for a bigger pool fire, this phenomenon becomes less obvious. This is mainly because of the repeated air entrainment happens in the sealed engine room. During the early stage of the experiment, the engine room can be filled with hot smoke very quickly after the ignition. Along the burning process, repeated air entrainment becomes much serious when more smoke is entrained. The phenomenon is much serious for a bigger pool, namely the fire with bigger size lessens the difference of the time to approach the maximum temperature at various heights. However, with a bigger pool, the temperature gradient becomes greater under a bigger fire size.

Fig. 4 shows that the time to reach the maximum temperature decreases with a bigger pool. It is known that the time of maximum temperatures occurred is close to the extinction time. In addition, it is observed from Fig. 4 that for the thermocouples positioned at different heights the times that they reach their maximum temperature are various to some extent.

Increasing trend of smoke temperature for large pool fire is much straightforward. This is much because of the smoke produced from the liquid fire source. For the pool fire with a relatively bigger diameter, more smoke can be produced which can spread over the whole sealed engine room during the test. The temperature in the sealed engine room can increase rapidly because of the hot smoke. This is also evidenced by Fig. 4 that the time to approach the maximum temperature drops from about 3813 s–670 s when the pool diameter rises from 10 to 35 cm.

There is little difference for the measured temperatures at ignition, which is because of the measurement accuracy caused by the thermocouple itself. The differences of initially measured temperatures at ignition for different thermocouples at various heights are within ± 1 °C. This kind of measurement accuracy is acceptable compared with the similar research activities (Dang et al., 2015). To minimize its influence, during data processing, temperature rises were calculated by deducting the initially measured temperature (ambient temperature at ignition) from the measured temperature at a later stage. The reason that a fixed ambient temperature was not used is that there is a variation of ± 1 °C for the initially measured temperature.

The variations in the obtained temperature rises along the height at different time are shown in Fig. 5. The change of temperature rises at different heights is defined as the gradient of temperature rise. It is seen that as the burning continues the gradient of temperature rise increases gradually. For each scenario shown in Fig. 5, the curve ends at the maximum temperature, showing the biggest temperature gradient. It is also obtained that the gradient of vertical temperature rise increases with a bigger pool. When the diameter of the pool pan increases from 10 to 30 cm, the gradient of vertical temperature rise approaches the maximum. However, the situation for 35 cm pool fire is exceptional, which is because of the decreased temperature gradient under a smaller average heat release rate. The details can be seen in Fig. 6.

The temperature rises at different heights at the time of maximum temperature for different diameter pool fires can also be obtained, as shown in Fig. 6. It is observed that the temperature rise increases under a higher height for all the tests. The temperature rises also show a very good linear relationship with the height. The slope of the linear relationship refers to the gradient of the temperature rises along the height. For a small pool fire, the temperature rises along the height change smoothly. The situation for a large pool fire is much different and that the temperature rise increases greatly along the height. For a 30 cm pool fire, its gradient of temperature rises is about 9 times of that of 10 cm pool fire.

The temperature gradient in the sealed room fire increases with a bigger pool fire, namely fire size. It can be seen from Fig. 6 that the temperature gradient increases when the pool size rises from 10 to 30 cm, showing a maximum temperature gradient of about 30 °C/m. Poulsen and Jomaas (2012) obtained a maximal temperature gradient of over 100 °C/m for the upper smoke layers under free burning pool fire in ISO 9705 test room, while Wang et al. (Wang et al., 2011; Ren et al., 2018) observed a maximal temperature gradient of about 55 °C/m for free burning polypropylene sheets in ISO 9705 test room. It can be known that the smoke layer of a fully sealed fire shows a similar or even a little lower temperature gradient than those of open fires.

4. Non-dimensional analysis of vertical temperature distribution at the time of maximum temperature

As mentioned in the introduction, the influence of the hot smoke released from the fire source on the engine room structure is worth being investigated, especially for the potential failure location under the high-temperature conditions. This is significant to the structural risk assessment and fire rescue. For the sealed engine room, the worst scenario is that the internal temperature approaches the maximum, which has the biggest impact on the related structure and components. In the following parts, a mathematical model is developed concerning this issue to benefit the engineering application.

4.1. Mathematical model

Following the similarity principle, fire characteristics in the reduced-scale model are consistent to those in the full-scale model. The non-dimensional analysis is a good method to eliminate the influences of scales, which is applicable to different scale tests. Therefore, a non-dimensional model will be developed to predict the vertical temperature rise distribution at the time of maximum temperature for sealed engine room fires.

Theoretically, the vertical temperature rise distribution $\Delta T(h)$ at time of the maximum temperature is determined by several factors, such as the average heat release rate ($\overline{Q}$), ambient temperature (T_∞), ambient air density (ρ_∞), specific heat capacity of ambient air (c_p), gravitational acceleration (g), vertical height (h), pool diameter (D), height of the sealed engine room (H), and the area of the sealed engine

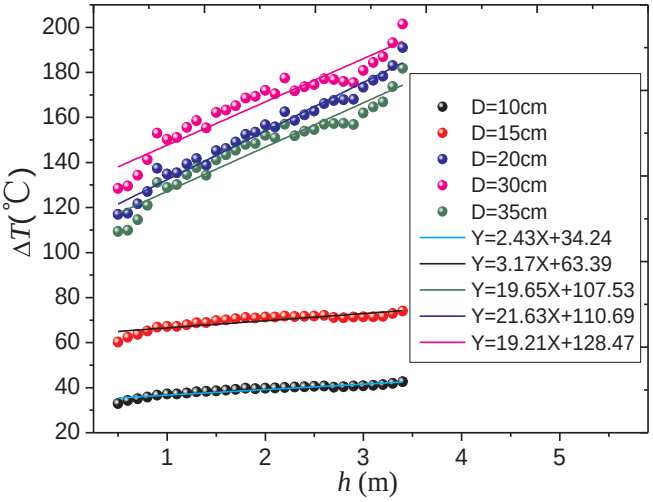

Fig. 6. The temperature rises at different heights at the time of maximum temperature for pool fires with various diameters.

room (S). The temperature rise along the height can then be given by,

$$\Delta T(h) = F(\bar{Q},\ T_\infty,\ \rho_\infty,\ c_p,\ g, h\ ,\ D,\ H,\ S) \tag{3}$$

Based on previous experimental and theoretical studies (Heskestad, 1975), non-dimensional *HRR* can be expressed by,

$$\dot{Q}^* = \frac{\dot{Q}}{\rho_\infty c_p T_\infty \sqrt{g} D^{5/2}} \tag{4}$$

As the heat release rate cannot be directly measured for a sealed engine room fire, its average *HRR* is defined as,

$$\bar{Q}^* = \frac{\bar{Q}}{\rho_\infty c_p T_\infty \sqrt{g} D^{5/2}} \tag{5}$$

To simplify Eq. (3), the dimensionless analysis is conducted. The variables including ρ_∞, T_∞, C_p, g, and D, are selected as fundamental variables of Eq. (3) before performing the dimensionless analysis. It should be noticed that in this study all experiments have been carried out only under the condition of constant geometric parameters of the ship engine room with an internal size of 3 m (Length) × 3 m (Width) × 3.5 m (Height). Thus, in this study, it means that H is not

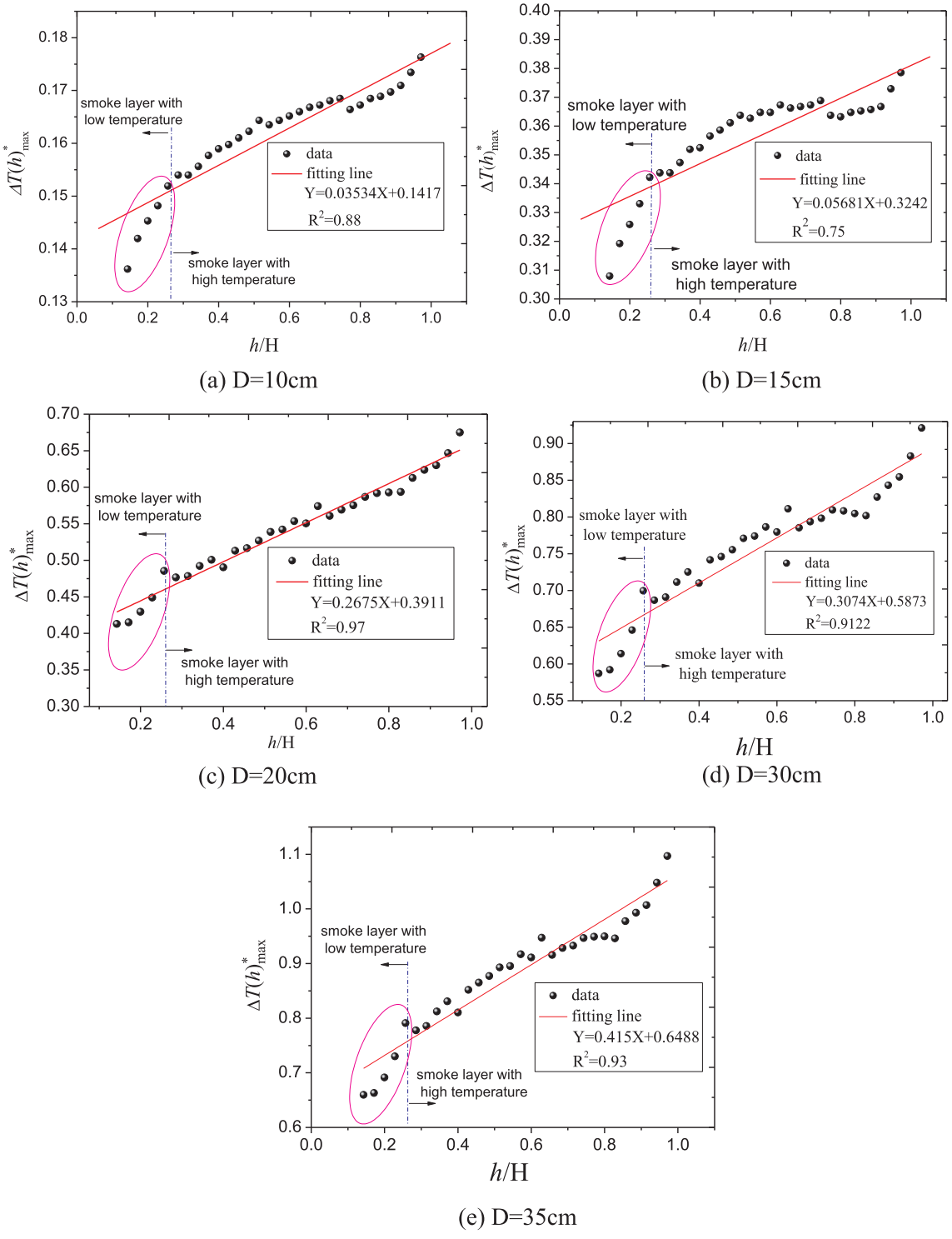

Fig. 7. Relationship between non-dimensional temperature rise and height.

independent on S, as shown in Eq. (3). So during the following dimensionless analysis, we have to choose one. Under the objective of investigating the vertical temperature rise, we choose to keep H in the following analysis rather than S. Certainly, the related experiments will be taken in our future work when the related test rig with various internal areas is available.

Kurioka et al. (2003) obtained a correlation between the maximum smoke temperature rise and transient heat release rate based on fire tests in various-scaled tunnel models. In this study, a relationship between the vertical temperature rise at the time of maximum temperature and average heat release rate is proposed with two considerations: (a) The transient *HRR* is very difficult to be measured directly because of the sealed test engine room; and (b) As shown in Fig. 2, the transient mass loss rate (be linear to heat release rate (Shi and Chew, 2013)) is very close to the average mass loss rate as there is no much variation during almost the whole burning period. Under these conditions, Eq. (3) can be normalized,

$$\frac{\Delta T(h)}{T_\infty} = F\left(\bar{\dot{Q}}^*, \ \frac{h}{D}, \frac{H}{D}\right) \tag{6}$$

Non-dimensional temperature rise can be defined as,

$$\Delta T(h)^*_{\max} = \frac{\Delta T_{\max}(h)}{T_\infty \bar{\dot{Q}}^*} \tag{7}$$

Substituting Eq. (7) into Eq. (6), it can be obtained that,

$$\Delta T(h)^*_{\max} = F_1\left(\frac{h}{D}, \ \frac{H}{D}\right) \tag{8}$$

Because D is selected as the characteristic length in this work, as also seen in Eq. (4), variables of h/D and H/D are independent. To obtain the non-dimensional temperature rise at different heights and ensure variables h/D and H/D are independent, the following equivalent operation is performed on Eq. (8),

$$F_1\left(\frac{h}{D}, \ \frac{H}{D}\right) \sim F_2\left(\frac{h}{H}, \ \frac{D}{H}\right) \tag{9}$$

Combining with Eqs. (6) and (9), the non-dimensional temperature rise at different heights is given by,

$$\Delta T(h)^*_{\max} = F_2\left(\frac{h}{H}, \ \frac{D}{H}\right) \tag{10}$$

In this study, a density of 1.2 kg/m^3 and specific heat capacity of 1.004 kJ/(kg·K) were selected for ambient air (Black et al., 2007; Baskut et al., 2010). The temperatures of ambient air are about 14–21 °C, as seen in Table 1.

Fig. 7 presents the relationship between non-dimensional temperature rise and height. It is known from this figure that the non-dimensional temperature rise shows a good linear relationship with non-dimensional height. The gradient of non-dimensional temperature rise increases with a bigger pool, which is consistent with the results shown in Fig. 6. However, it needs to be noticed that there are two smoke regions with high and low temperature, respectively, for each test by a vertical diving line with a non-dimensional height of about 0.3. As the diameter of pool increases, the non-dimensionless vertical temperature rise is more linearly correlated with the dimensionless height. For pool fires with different diameters, those intercepts from the regression are different. To address the influences of D/H on slope k and intercepts b, the following linear relationship is assumed,

$$\Delta T(h)^*_{max} = k\frac{h}{H} + b \tag{11}$$

Based on the regression between D/H and k, as shown in Fig. 8, it can be seen that k shows a good linear relationship with D/H with a coefficient of determination of 0.9042, which is given by,

$$k = 5.289\frac{D}{H} - 0.116 \tag{12}$$

Similarly, the intercept b gives a good linear relationship with D/H with the goodness of fit of 0.9735, as shown in Fig. 9, which can be expressed by,

$$b = 6.822\frac{D}{H} - 0.01 \tag{13}$$

Combining Eqs. 11–13, the non-dimensional temperature rise can be predicted by,

$$\Delta T(h)^*_{\max} = \left(5.289\frac{D}{H} - 0.116\right)\frac{h}{H} + 6.822\frac{D}{H} - 0.01 \tag{14}$$

5. Discussion

The vertical distribution profile of the temperature in a sealed ship engine room was investigated in this study, which is certainly different from those open fires in the literature. From the experimental results during the early stage, smoke quickly fills the whole engine room after the ignition. After that, the repeated air entrainment happens in the sealed engine room and smoke temperature eventually forms a top-down vertical distribution in the space after the self-extinction of fire. The temperature gradient in the vertical direction is slightly smaller than that in a compartment with opening(s). As the air inlet and outlet are closed, the fresh air outside is prevented from entering the engine room, which directly affects the fire combustion process in the sealed engine room.

After a period of combustion after ignition, the fire development is mainly dominated by the oxygen concentration in the engine room. As for the fire behaviors, such as temperature, the application of traditional zone fire model is still available. It can be roughly considered that the smoke layer is divided into the top high-temperature layer and the bottom low-temperature layer. However, from the view of the thermal stress safety of ship engine room structure, this temperature gradient cannot be ignored because different temperature rises can cause local structural stress differences for ship engine room.

It should be noted that the experimental study in this paper mainly considers the case of fire source centrally located at the bottom of ship engine room. The other cases of fire sources located with different heights or different horizontal positions, such as the corner fire or wall fire, were not covered in this study. Obviously, the results of these cases would be different to that in this study.

Due to limited experimental conditions, the geometric shape variation is not considered in this paper, namely a parameter of S/H^2 with

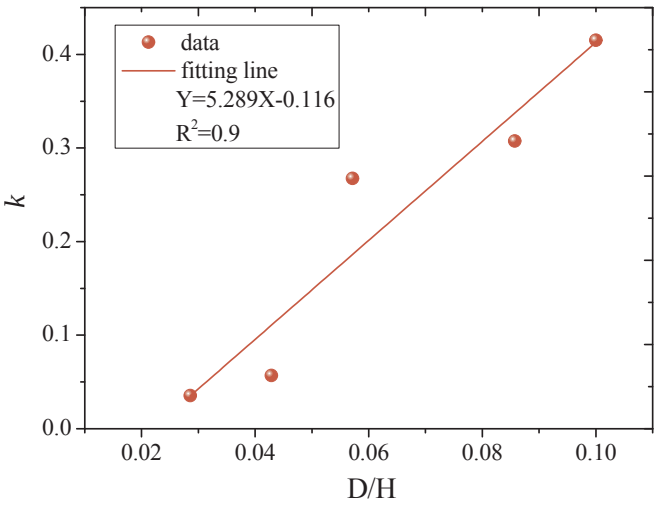

Fig. 8. The relationship between slope k and D/H.

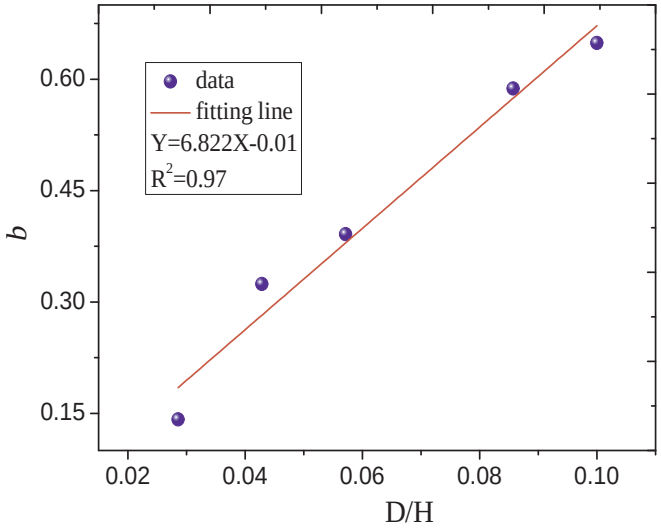

Fig. 9. The correlation between intercept b and D/H.

a constant of 0.734. It should be noted that this parameter is correlated to the functional form of vertical temperature distribution. The model developed in this study is not applicable to the engine room with a largely changed S/H^2 in comparison with it in this article. The future work will focus on the related experimental investigations under the available experimental rig.

6. Conclusions and future work

Sealed ship engine room fire is conducted both experimentally and non-dimensionally based on a bench-scale engine room with a dimension of 3 m (Length) × 3 m (Width) × 3.5 m (Height). The main purpose of this work has been focused on the vertical distribution of temperature induced by fire in a sealed ship engine room. Some conclusions can be addressed:

(1) It is known from experiments that the burning time decreases for pool fire with a small diameter, and the time to approach the maximum temperature is near the experiment end. The time to reach a maximum temperature at different heights is different. With a lower height, the time to approach the maximum temperature rise is longer with a more obvious air entrainment and thermal buoyancy. The vertical temperature rise also shows a good relationship with height. The gradient of temperature rise increases with pool diameter that the gradient of temperature rise for a 30 cm pool fire is about 9 times of that of a 10 cm pool fire.
(2) For sealed engine room fires, experimental results demonstrated that the smoke temperature along the height is not identical, showing an obvious gradient along the height. The smoke layer of a fully sealed fire shows a similar or even a little lower temperature gradient than that of open fires. The gradient of temperature rise of a 30 cm pool fire is about 9 times of that of a 10 cm pool fire. Meanwhile, the experimental results demonstrate that the time to reach the maximum temperature is different for smoke layers at various heights, while a lower height shows a relatively long delay time.
(3) The average heat release rates of pool fires with different diameters in this study are within 2.6–34.1 kW, which is corresponding to 470.7–6155 kW fires in the full-scale ship engine room of 24 m (Length) × 24 m (Width) × 28 m (Height). A non-dimensional model was developed to predict the vertical temperature rise at the time of maximum temperature for pool fires in a sealed engine room,

$$\Delta T(h)^*_{\max} = \left(5.289\frac{D}{H} - 0.116\right)\frac{h}{H} + 6.822\frac{D}{H} - 0.01$$

It needs to be noted that due to the limited experimental conditions the geometric shape parameter, S/H^2, is not included in the mathematical model of vertical temperature distribution developed in this paper. The future work should be made to build more experimental platforms with different geometric shapes and conduct relevant experimental studies.

Acknowledgment

The authors would like to thank the anonymous reviewers and the editor-in-chief for their constructive suggestions for improving this paper. This work was financially supported by the National Natural Science Foundation of China (Grant No.: 50909058, 71503166, and 51109127), Natural Science Foundation of Shanghai (Grant No. 16ZR1414600), and Shanghai Sailing Program (Grant No. 18YF1409600).

References

Baskut, O., Ozgener, O., Ozgener, L., 2010. Effects of meteorological variables on exergetic efficiency of wind turbine power plants. Renew. Sustain. Energy Rev. 14 (9), 3237–3241.
Black, A., Hobbs, M.L., Dowding, K.J., Blanchat, T.K., 2007. Uncertainty quantification and model validation of fire/thermal response predictions. In: The 18th AIAA Computational Fluid Dynamics Conference, Miami, USA.
Bonte, F., Noterman, N., Merci, B., 2013. Computer simulations to study interaction between burning rates and pressure variations in confined enclosure fires. Fire Saf. J. 62 (62), 125–143.
CB/T3368-2013, 2013. Typical Fire-proof Structure of Hull Fire Prevention Division. China State Shipbuilding Corporation.
Chen, B., 2011. Experimental Study on Pool Fire Environment in Ship Room with Ceiling Vent. Ph.D. Thesis. University of Science and Technology of China, Hefei, China.
Chen, B., Lu, S.X., Li, C.H., Kang, Q.S., Lecoustre, V., 2011. Initial fuel temperature effects on burning rate of pool fire. J. Hazard Mater. 188 (1), 369–374.
Dang, G.X., Zhong, F.Q., Zhang, Y.J., Zhang, X.Y., 2015. Numerical study of heat transfer deterioration of turbulent supercritical kerosene flow in heated circular tube. Int. J. Heat Mass Tran. 85, 1003–1011.
Heskestad, G., 1975. Physical modeling of fire. J. Fire Flammability 6, 253–273.
Hu, Z.X., Utiskul, Y., Quintiere, J.G., Trouve, A., 2005. A comparison between observed and simulated flame structures in poorly ventilated compartment fires. Fire Saf. Sci. 8, 1193–1204.
Hu, J., Lu, S.X., Li, C.H., 2010. A study on temperature characteristic in enclosed cabin fire. fire safety sci 19 (3), 109–115.
Jia, F., Galea, E.R., Patel, M.K., 1997. The prediction of fire propagation in enclosure fires. In: The Fifth International Symposium on Fire Safety Science, Melbourne, Australia, pp. 439–450.
Jin, D.H., 2012. Large eddy simulation of an airtight chamber fire. Fire Sci. Technol. 31 (5), 463–466.
Jin, Y.L., Jang, B.S., 2015. Probabilistic fire risk analysis and structural safety assessment of FPSO topside module. Ocean Eng. 104, 725–737.
Jin, Y.L., Jang, B.S., Kim, J.D., 2016. Fire risk analysis procedure based on temperature approximation for determination of failed area of offshore structure: living quarters on semi-drilling rig. Ocean Eng. 126, 29–46.
Kang, H.J., Jin, C., Lee, D., Park, B.J., 2017. A framework for using computational fire simulations in the early phases of ship design. Ocean Eng. 129, 335–342.
Kim, S.J., Lee, J., Kim, S.H., Sohn, J.M., 2017. Nonlinear structural response in jet fire in association with the interaction between fire loads and time-variant geometry and material properties. Ocean Eng. 144, 118–134.
Kurioka, H., Oka, Y., Satoh, H., Sugawa, O., 2003. Fire properties in near field of square fire source with longitudinal ventilation in tunnels. Fire Saf. J. 38 (4), 319–340.
Li, C.H., 2010. Experimental Study on Pool Fire Behaviors in Closed Compartment on Ship. Ph.D. Thesis. University of Science and Technology of China, Hefei, China.
Li, C.H., Lu, S.X., Yuan, M., Zhou, Y., 2010. Studies on ghosting fire from pool fire in closed compartments. J. Uni. Sci. Tech. China 40 (7), 751–756.
Li, Q.X., Li, Y., Liu, H., 2011. Analysis of smoke flow characteristics of submarine fire under closed-compartment conditions. J. Nav. Univ. Eng. 23 (5), 64–67.
Li, Q., Zhang, J.Q., Li, J.M., Zhang, B.S., Jiang, Y., 2018. Combustion phenomena of pool fire in a ceiling vent compartment: the vent far away from the fire source. Procedia Eng 211, 388–394.
Liu, X.Y., Xu, S.L., Lu, S.X., Li, Y.L., 2004. Analysis and design of similarity model of ship fire simulation engine room. Fire Sci. Technol. 23, 413–417.
Ma, T.G., 2015. Ignitability and Explosibility of Gases and Vapors. Springer, New York.
Poulsen, A., Jomaas, G., 2012. Experimental study on the burning behavior of pool fires in rooms with different wall linings. Fire Technol. 48 (2), 419–439.
Pu, J.Y., 2009. Warship Survivability. National Defense Industry Press, Beijing.
Ren, F., Hu, L.H., Sun, X.P., Hu, K.Z., 2018. An experimental study on vertical temperature profile of facade fire plume ejected from compartment with an opening

subjected to external wind normal to facade. Int. J. Therm. Sci. 130, 94–99.
Roh, J.S., Yang, S.S., Ryou, H.S., Yoon, M.O., Jeong, Y.T., 2008. An experimental study on the effect of ventilation velocity on burning rate in tunnel fires - heptane pool fire case. Build. Environ. 43 (7), 1225–1231.
Salem, A.M., 2013. Parametric analysis of a cabin fire using a zone fire model. Alexandria Eng. J. 52 (4), 627–636.
Salem, A.M., 2016. Use of Monte Carlo Simulation to assess uncertainties in fire consequence calculation. Ocean Eng. 117, 411–430.
Sekret, R., Saleta, D., Sztarbala, G., Smardz, P., 2013. Comparison of CFD modeling with fire tests, Comparison of CFD modelling with results of full scale compartment fire test in a residential unit. In: International Conference on Application of Structural Fire Engineering, Prague, Czech Republic.
Shi, L., Chew, M.Y.L., 2012. Influence of moisture on autoignition of woods in cone calorimeter. J. Fire Sci. 30 (2), 158–169.
Shi, L., Chew, M.Y.L., 2013. Fire behaviors of polymers under autoignition conditions in a cone calorimeter. Fire Saf. J. 61 (4), 243–253.
Su, S.C., Wang, L., 2013. Three dimensional reconstruction of the fire in a ship engine room with multilayer structures. Ocean Eng. 70 (5), 201–207.
Su, S.C., Wang, L., Nie, Y.H., Gu, X., 2012. Numerical computation and characteristic analysis on the center shift of fire whirls in a ship engine room fire. Saf. Sci. 50 (1), 12–18.
Sugawa, O., Kawagoe, K., Oka, Y., Ogahara, I., 1991. Burning behavior in a poorly-ventilated compartment fire-ghosting fire. Nucl. Egn. Des 125 (3), 347–352.
Tatem, P.A., Williams, F.W., Ndubizu, C.C., Ramaker, D.E., 1986. Influence of complete enclosure on liquid pool fires. Combust. Sci. Technol. 45 (3–4), 185–198.
Trouve, A., Wang, Y., 2010. Large eddy simulation of compartment fires. Int. J. Comput. Fluid Dynam. 24 (10), 449–466.
Utiskul, Y., Quintiere, J.G., Rangwala, A.S., Ringwelski, B.A., Wakatsuki, K., Naruse, T., 2005. Compartment fire phenomena under limited ventilation. Fire Saf. J. 40 (4), 367–390.
Walton, W.D., Thomas, P.H., Ohmiya, Y., 2016. Estimating temperatures in compartment fires. In: Hurley, M.J., Gottuk, D.T., Hall Jr.J.R., Harada, K., Kuligowski, E.D., Puchovsky, M., Torero, J.L., Watts Jr.J.M., Wieczorek, C.J. (Eds.), SFPE Handbook of Fire Protection Engineering. National Fire Protection Association, Quincy, Massachusetts, pp. 1002–1010.
Wang, X.G., Cheng, X.D., Li, L.M., Lo, S.M., Zhang, H.P., 2011. Effect of ignition condition on typical polymer's melt flow flammability. J. Hazard Mater. 190 (1), 766–771.
Wang, J.H., Chu, G.Q., Li, K.Y., 2013. Study on the uncertainty of the available time under ship fire based on Monte Carlo sampling method. China Ocean Eng. 27 (1), 131–140.
Wang, J.H., Li, G.Q., Shi, L., Jiao, Y., Xie, Q.M., 2017. Transport time lag effect on smoke flow characteristics in long-narrow spaces. Fire Technol. 53 (3), 983–1010.
Yang, F., Pu, J.Y., Li, Q.X., Wu, X.J., 2013. Characteristics of temperature distribution of pool fires in closed cabin. J. Nav. Univ. Eng. 25 (3), 61–65.
Yao, Y.Z., Cheng, X.D., Zhang, S.G., Zhu, K., Zhang, H.P., Shi, L., 2017. Maximum smoke temperature beneath the ceiling in an enclosed channel with different fire locations. Appl. Therm. Eng. 111, 30–38.
Yoon, S.S., Figueroa, V., Brown, A.L., Blanchat, T.K., 2010. Experiments and modeling of large-scale benchmark enclosure fire suppression. J. Fire Sci. 28 (2), 109–139.
Yuan, M., Lu, S.X., Zhou, Y., Zhang, J.Q., 2014. A simplified mathematical model for predicting the vertical temperature profiles in enclosure fires without vertical opening. Fire Technol. 50 (4), 929–943.
Zhang, J.Q., 2014. Fire Dynamics in Ship Enclosures Considering the Effects of Ceiling Vent and Fire Locations. Ph.D Thesis. University of Science and Technology of China, Hefei, China.
Zhang, J.Q., Lu, S.X., Li, Q., Yuen, R., Yuan, M., Li, C.H., 2013a. Impacts of elevation on pool fire behavior in a closed compartment: a study based upon a distinct stratification phenomenon. J. Fire Sci. 31 (2), 178–193.
Zhang, J.Q., Lu, S.X., Li, C.H., Yuan, M., Yuen, R., 2013b. On the self-extinction time of pool fire in closed compartments. Procedia Eng 62, 266–274.
Zhang, S.G., Ni, X.M., Zhao, M., Feng, J.J., Zhang, R.F., 2015. Numerical simulation of wood crib fire behavior in a confined space using cone calorimeter data. J. Therm. Anal. Calorim. 119 (3), 2291–2303.